U. S. DEPARTMENT OF THE INTERIOR
U. S. GEOLOGICAL SURVEY

CROSSWELL RADAR: A FEASIBILITY TEST AT THE M-AREA SETTLING BASIN, SAVANNAH RIVER SITE, SOUTH CAROLINA

by

Karl J. Ellefsen[1]

Open-File Report 97–144

---

[1] U. S. Geological Survey, MS 964, Box 25046, Denver, CO 80225

1997

ABSTRACT

At the M-Area Settling Basin, Savannah River Site, the unsaturated and the saturated zones have been contaminated with dense non-aqueous phase liquids. To decrease the cost of remediating the contaminants, some means of monitoring the remediation within the ground is needed. One promising technology is crosswell radar. Because the electromagnetic properties of the sediments and the well grout could prevent the method from being suitable for monitoring, a feasibility test was performed. The test involved the interpretation of crosswell radar data that were collected between the five wells on the north side of the M-Area Settling Basin.

In the unsaturated zone, three statistical relations were developed by comparing the radar data, which were collected between wells MSB-3A and MSB-3B, to the average percentage of clay-size particles, which were measured in core extracted from well MSB-3B: (1) Where radar waves are present in the scans, the median percentage is 10. (2) Where radar waves are absent from the scans, the median percentage is 38. (3) The slowness of the radar waves is positively correlated to the logarithm of the percentage; the correlation coefficient (r) is 0.77. Using these three relations, the percentages of clay-size particles were predicted across the entire well cluster. These predictions show that the sediments are horizontally-layered and that the composition of the layers sometimes changes in the horizontal direction.

In the saturated zone, two statistical relations were developed by comparing the radar data, which were collected between wells MSB-3C and MSB-3B, to the average percentage of clay-size particles, which were measured in core extracted from well MSB-3B: (1) Where radar waves are present in the scans, the median percentage is 9. (2) Where radar waves are absent from the scans, the median percentage is 23. These two relations in conjuction with forward modeling were used to interpret the radar scans between 144 and 158 ft (depth), an interval contaminated with dense non-aqueous phase liquids. The results indicate that the sediments within this interval are horizontally-layered.

The findings of this feasibility test clearly show that crosswell radar data can be collected near the M-Area Settling Basin and that the attributes of the radar waves are strongly related to the geology. It is still not known, however, whether this method can be used to monitor remediation; this can be determined only with a field test.

CONTENTS

LIST OF FIGURES

LIST OF TABLES

1. INTRODUCTION

At Savannah River Site, which is near Aiken, South Carolina, approximately 2 million pounds of dense non-aqueous phase liquids (DNAPLs) were put into the M-Area Settling Basin (Westinghouse Savannah River Company, 1992, p. 2) from which they migrated into the unsaturated and the saturated zones. To decrease the cost of remediating the contaminated sediments, the progress of the remediation must be monitored (Jordan and others, 1993). It might be possible to perform this monitoring with a geophysical method, which has the notable advantage of being non-intrusive. The most appropriate geophysical method is not known, and so different methods were tested at the Site by the U. S. Geological Survey.

Because the electromagnetic properties of DNAPLs, surfactants (including alcohol), and water are significantly different from each other, a geophysical method that can detect these differences might be suitable for monitoring. One such method is ground penetrating radar, which has been used to monitor the migration of DNAPLs in saturated, unconsolidated sediments (Greenhouse and others, 1993). However, ground penetrating radar is inappropriate for monitoring remediation near the Basin because the clay layers, which are prevalent, would completely attenuate the radar waves.

Another method that might be suitable for monitoring is crosswell radar. To collect crosswell radar data, an antenna in one well is used to generate a radar wave, and another antenna in a nearby well is used to detect the wave as it passes. However, the sediments or the well grout could attenuate the radar waves so much that the waves would be undetectable. Consequently, a feasibility test was performed: Crosswell radar data were collected within the unsaturated and the saturated zones near the Basin, and the data were interpreted to determine how they were affected by the sediments and the wells. The findings of this test show the potential of crosswell radar for monitoring remediation.

2. GEOLOGY AND WELL CONSTRUCTION

Savannah River Site is in the Atlantic Coastal Plain; within about 200 ft (60 m) of the surface, the zone pertinent to this investigation, the sediments consist of unconsolidated clays, silts, sands, and gravels that were deposited in shallow marine, lagoonal, fluvial, and flood plain environments. (Westinghouse Savannah River Company, 1992, p. 18; Eddy-Dilek and others, 1993, p. 11). The sediments are horizontally-layered, and the composition of a layer sometimes changes laterally. The clay consists almost entirely of kaolinite, although in some layers illite and smectite are present in small quantities (DiStefano, 1989; Seagull, 1992; Horton, 1996). When the radar data were collected, the elevation of the water table was 232 ft (71 m).

The wells in which the data were collected are on the north side of the M-Area Settling Basin (Figure 1). The five wells are roughly along an east-west line, are separated from each other by about 15 ft (5 m), are straight and vertical (Ellefsen, 1995), and extended to different depths (Figure 2). The casing and screen are polyvinyl chloride plastic with an

inside diameter of 4 in (0.10 m); they are anchored to the sediments with grout, sand pack, or gravel pack, which are all about 7 in (0.18 m) thick.

3. DATA COLLECTION AND DATA PROCESSING

The data were collected during June 1994. For the unsaturated zone, the measurements were between adjacent wells — for example, between wells MSB-22 and MSB-3D. For the saturated zone, the measurements were only between wells MSB-3C and MSB-3B because the other wells that penetrated the saturated zone significantly, MSB-22 and MSB-3D, are contaminated with a small amount of polychlorinated biphenyl, which is dissolved in the DNAPL (J. Rossabi, oral commun., 1997). Most of the data presented here are zero-offset: the difference between the elevations of the two antennas was zero. A detailed summary of all zero-offset data is in Table 1.

The electronic equipment used to collect the data consisted principally of the radar control unit (Geophysical Survey Systems, Inc., 1993) and the borehole antennas, which were built by the U. S. Geological Survey. The equipment settings used to collect the data are summarized in Table 2. The duration of each scan and the time at which it started were selected to make the recorded wave in the middle third of the scan. Because the data cannot be filtered before digitization, the sample rate was set very high to minimize the amount of high frequency, ambient noise being aliased into the radar signal. The parameters for the bandpass filter were selected to pass those frequency components at which the radar waves had high amplitudes — the passband always included the center frequency of the antennas, which is 200 MHz if the antennas are in air, as well as lower frequencies. Determining suitable receiver gains was difficult because the amplitude of the wave, if the wave was detectable at all, was significantly affected by the lithology (see sections 4 and 5). To set the gains, this procedure was found to work satisfactorily: (1) Zero-offset data were collected to find where the amplitude was the highest. (2) For that interval, the gain was set to make the recorded amplitudes high, yet still low enough to prevent saturation of the digitizer.

The processing consisted of two steps. First, the gain was removed from each scan. Second, the scans were filtered with a zero-phase bandpass filter to minimize the random noise; the passband ranged approximately from 80 to 300 MHz, which was broad enough to include the radar signal.

The radar scans are displayed in a cross section (Figure 2). Because all five wells are close to the cross section, the distortion of the scans caused by the projection is negligible. Each scan is plotted with its beginning on the left, at the location of the transmitting antenna, and its end on the right, at the location of the receiving antenna. (The transmitting antenna was always in the left well, and the receiving antenna was always in the right well (Table 1).) All scans between one pair of wells are scaled equally to show the relative amplitudes of the waves, and the scale factor is written just above the top scan. For example, the scale factor for all scans between wells MSB-22 and MSB-3D is 2.2. The scale factors are different for each pair of wells, and so, if data from different pairs of wells

are being compared, the amplitudes must be divided by these scale factors. (The anomalously large scale factor for the data between wells MSB-3C and MSB-3A was probably caused by a problem with a cable. Because of the large scale factor, an electronic signal at the beginning of the scans is noticeable.) The gamma ray logs, which were provided by Westinghouse Savannah River Company, are plotted with the high values on the right. These logs indicate the abundance of illite but not kaolinite, the most prevalent clay mineral near the M-Area Settling Basin. The log of the percentage of clay-size particles, which was also provided by Westinghouse Savannah River Company, is from microscopic measurements of core extracted from well MSB-3B. A clay-size particle has a diameter less than 2.25×10^{-3} in (0.0625 mm) (Environmental Sciences Section, 1993).

4. RESULTS FOR THE UNSATURATED ZONE

4.1 Interpretation

The interpretation for the unsaturated zone is based on statistical relations between the percentages of clay-size particles and attributes of the radar waves. First, these relations will be developed, and then they used to interpret the data.

In most scans between wells MSB-3A and MSB-3B (Figure 2), a radar wave is present; in a few scans, it is absent. (In this report, "present" is defined as being distinguishable from the background noise in the scan; "absent" as being indistinguishable.) To determine whether there is any relation between the presence (or the absence) of a radar wave and the percentage of clay-size particles, histograms for each case were constructed. The percentages were averaged over 3 ft (0.9 m) intervals because with such averaging the locations of the measurements could be matched to the locations of the scans and because the averaging accounts somewhat for the different scales of measurement (see section 4.2). The two histograms (Figure 3) differ markedly: If the wave is present, the percentage tends to be low — the median is 10. In contrast, if the wave is absent, the percentage tends to be high — the median is 38. The percentage that appears to separate the two cases is about 25. Assuming that the percentage of clay-size particles is related to the amount of mineralogical clay, these histograms reflect a thoroughly documented property of radar wave propagation: clays attenuate radar waves (see, for example, Daniels, 1989; Davis and Annan, 1989).

In those scans between wells MSB-3A and MSB-3B for which a radar wave is present (Figure 2), the traveltimes vary significantly. To determine whether there is any relation between the traveltimes and the percentage of clay-size particles, a scatter plot was constructed. The traveltime was picked at the first trough (negative peak) in the radar wave because this pick is more accurate than that for the first arrival. Then the traveltime was converted to slowness to remove the effect of the distance between the wells. The scatter plot (Figure 4a) indicates that the slowness is positively correlated with the logarithm of the percentage of clay-size particles. The sample correlation coefficient (r) is 0.77, indicating that the correlation is moderate. The likely explanation for this correlation is that the partial saturation, and hence the dielectric permittivity, increases as the amount

of fine-grained sediment increases — near the M-Area Settling Basin, the partial saturation is higher in the fine-grained sediments than it is in the coarse-grained sediments (Nelson and Kibler, 1995).

A straight line was fit to the points in the scatter plot using classical linear regression (Devore, 1982, p.422–458). To prevent this line from being adversely affected by the outlier, whose logarithm and slowness are 1.11 and 9.84 ns/m, respectively, the outlier was omitted from the regression. The residuals were normalized (Figure 4b) by dividing them by the sample standard deviation (Devore, 1982, p. 460). Because the residuals show no trend and are within two (normalized) standard deviations of the mean (zero), the straight line is a suitable model for the data. Moreover, the variance in the normalized residuals is approximately constant for all values of the logarithm — this constancy was the reason for the logarithmic transformation (Neter and others, 1983, p. 132–137).

This regression line may be used to predict, in an inverse sense, a logarithm for a specified slowness (Neter and others, 1983, p. 172). The inverse prediction interval (Figure 4a) shows the range of plausible values for the logarithm. For example, if the slowness is 10 ns/m, then the plausible values are between 0.56 and 0.94. The level for the inverse prediction interval was chosen to be 80%, a low value, because different volumes of sediment and different scales of measurement are being related (see section 4.2). The interval is reasonable everywhere except for slownesses greater than 14 ns/m: the largest percentages within the interval are greater than 25, which are so large that the wave would probably be absent from the scan (see Figure 3b). Because of the width of the inverse prediction interval, two predicted logarithms must differ alot for there to be much confidence that the sediments are indeed different.

Using this regression line, logarithms of the percentages were predicted across the entire well cluster (Figure 5). Each prediction, which was made wherever a radar wave is present, is represented by a rectangle whose width equals the spacing between the wells and whose height equals the spacing between successive locations of the antennas. To help interpret these predictions, the average percentage of clay-size particles from the core measurements is also displayed.

Wherever a radar wave is absent, the histogram for absent waves (Figure 3b) indicates that the percentage is probably greater than about 25. Making such a prediction with the histogram requires some justification. The histogram was constructed from the data between wells MSB-3A and MSB-3B, and these data were affected by the distance between these two wells. This distance is practically equal to those between the other wells, and so the effect of distance on attenuation is practically the same for all radar scans. The data between wells MSB-3A and MSB-3B were also affected by the electromagnetic properties of the grout around these two wells. The well construction records (C. Eddy-Dilek, unpub. data, 1995) indicate that the amount of bentonite added to the grout differs slightly for each well, and so the attenuation caused by the grout will differ slightly (see section 4.2). This variation will introduce some error into the prediction. Nonetheless, the absences of radar waves, in all but one case, are within or

adjoining layers having a high percentage of clay-size particles (Figure 5), and so the predictions that these absences are related to high percentages are probably correct.

A typical layer with moderate to high percentages of clay-size particles (Figure 5) is between 39 and 68 ft (12 and 21 m) depth. At some locations within this layer the radar wave is absent; here the percentage of clay-size particles is probably greater than 25. Also, the percentages within this layer are not constant. A typical layer with low percentages is between 106 and 121 ft (32.5 and 37.0 m) depth. Again, the percentages within this layer are not constant. (Between 106 and 113 ft (32.5 and 34.5 m) depth, the percentages measured in core were too sparse to compute an average percentage. Little core was recovered probably because the sediments lacked cohesion, which comes from clay.) The layers at other depths may be interpreted in a similar manner. These examples show that the sediments are horizontally-layered and that the composition of the sediments sometimes changes in the horizontal direction; this interpretation is consistent with the known geology (see section 2).

4.2 Discussion of Interpretation

The distributions in the two histograms (Figure 3) overlap slightly, and the data points in the scatter plot (Figure 4a) are moderately scattered. The overlap and the scatter are caused by at least three phenomena: (1) The radar waves and the measurements of the percentage are at different spatial scales. The radar waves are strongly affected by the properties of the sediments within the first Fresnel zone (Born and Wolf, 1980, p. 370–375), which, at the well with receiving antenna, was approximately 3 ft (1 m) in diameter for the dominant frequency. In contrast, the measurements of the percentages were from sections of core that were 1 ft (0.3 m) long. I am unaware of any rigorous method to compare measurements at different spatial scales, and so I used an arithmetic average. (2) The radar waves and the measurements of the percentage pertain to different volumes. The radar waves were affected by the properties of the sediments between wells MSB-3A and MSB-3B, whereas the percentages were measured from core extracted from well MSB-3B. The compositions of these two volumes differ; evidence in support of this claim is difference between the two gamma ray logs, which were collected in wells only about 60 ft (18 m) apart (Figure 2). (3) The radar waves were affected differently by different minerals, but the percentages include all minerals that satisfy the size criterion (see section 3). For example, radar waves are strongly attenuated by clays but weakly attenuated by quartz; the percentages include clay as well as fine-grained quartz.

The overlap in the two histograms (Figure 3) and scatter in the scatter plot (Figure 4a) are two sources of error in the interpretation. Another source of error is the low amplitudes of the radar waves recorded between wells MSB-22 and MSB-3D and between wells MSB-3D and MSB-3C (Figure 2). (These low amplitudes are probably caused by the electromagnetic properties of the grout.) Even though the amplitudes of the waves are low, the background, random noise is not (see section 6). The consequence is that it is sometimes difficult to determine whether a wave is present, and, if the wave is, it is sometimes difficult to pick its traveltime. (For this reason, the percentage could not be

predicted between wells MSB-3D and MSB-3C from 79 ft (24 m) to 89 ft (27 m) depth.) Despite these sources of error, the predictions of the percentage are consistent with the known geology.

5. RESULTS FOR THE SATURATED ZONE

5.1 Interpretation

The interpretation for the unsaturated zone was based mostly on the correlation between the slowness (or equivalently traveltime) and the percentage of clay-size particles. Such a pronounced correlation, however, does not exist for the saturated zone — the traveltimes are roughly constant even though the percentage of clay-size particles changes markedly (Figure 2). Consequently, a different method must be used to interpret the data: First, histograms of the percentage of clay-size particles will be constructed. Then, these histograms along with traveltimes, amplitudes, and percentages of clay-size particles will be used to interpret the data between 144 and 158 ft (44 and 48 m) depth; this zone is particularly important because it is contaminated with DNAPL.

In most scans between wells MSB-3C and MSB-3B (Figure 2), a radar wave is present; in a few scans, it is absent. Histograms of the percentages were constructed exactly as those for the unsaturated zone were. Again, the two histograms (Figure 6) differ markedly: If the wave is present, the percentage tends to be low — the median is 9. In contrast, if the wave is absent, the percentage tends to be high —the median is 23. The percentage that appears to separate the two cases is about 20. The likely explanation for these two different distributions is that the percentage of clay-size particles is related to the amount of mineralogical clay, which attenuates the radar wave.

The zone from 144 ft (44 m) to 158 ft (48 m) depth may be divided into three intervals according to the behavior of the radar waves (Figure 7a). In intervals 1 and 3, radar waves are absent from the scans. Generally, the measured percentage of clay-size particles is high — this observation is consistent with the histogram for absent waves (Figure 6b). An exception is in the lower part of interval 1: the measured percentage may not be representative of that between the wells.

In interval 2 (Figure 7a), radar waves are present in the scans. The measured percentage of clay-size particles is low to moderate — this observation is consistent with the histogram for present waves (Figure 6a). Additional information about the waves is in the traveltime, which, for this investigation, is defined as the time at the first trough (negative peak) in the wave. The traveltime changes systematically with depth: it is high at the top, low in the middle, and moderately high at the bottom. This trend is similar to the trend for the percentage of clay-size particles (Figure 7c): the percentage is moderate at the top, low in the middle, and moderate again at the bottom. Assuming that the percentage of clay-size particles is related to the amount of mineralogical clay, this similarity indicates that mineralogical clay affects the dielectric permittivity. The effect, however, is small

because the change in the traveltime is small, merely 2 ns. (For this reason, the effect is not readily apparent in the data from the entire saturated zone (Figure 2).)

It is tempting to correlate the amplitude and the percentage of clay-size particles, but analyzing the data in this manner would probably be incorrect because the correlation would not account for reflected and refracted waves, which can be caused by geologic features at depths different from that of the radar scan. For example, in the scan at 155 ft (47.25 m) depth, the radar wave may include of a wave reflected from the layer at 157 ft (48 m), which has a high percentage of clay-size particles. Indeed, the strong effect that multiply-reflected (guided) waves have on amplitudes, but not on traveltimes, was observed in a numerical study of radar wave propagation in layered sediments (Ellefsen, 1996).

The interpretation of the data, especially that from interval 2, was refined with forward modeling; the advantage of forward modeling is that amplitudes can be properly interpreted because all waves, including reflected and refracted waves, are calculated. The model was chosen to be a stack of horizontal, homogeneous layers because the sediments were deposited in horizontal layers that are usually continuous over large areas (see section 2). The top and the bottom layers of the stack are half-spaces. The number of layers was chosen to be the number of radar scans. The thickness of each layer equals the spacing between successive scans (see Table 2), and the middle of each layer is centered on a scan. Each layer is isotropic, and its constitutive parameters are linear and independent of frequency. Although frequency independence is difficult to justify because the dielectric permittivity of typical soils and sediments is known to depend upon frequency (see, for example, Hoekstra and Delaney, 1974), this idealization was used anyway because it greatly reduces the number of model parameters. The transmitting antenna is simulated by a vertical electric dipole that has infinitesimal length. For the receiving antenna, the vertical component of the electric field intensity, the same component sensed by the antenna, is calculated. The wells are omitted from the model. The formulae by which the scans are calculated are derived in the Appendix.

To match the calculated and the field scans, constitutive parameters for each layer and the current in the dipole had to be selected. A different relative dielectric permittivity was chosen for each layer. The electrical conductivity was chosen to be a function of the relative dielectric permittivity:

$$\sigma = 10^{\varepsilon_r - 223} \text{ (S/m)} \tag{1}$$

where σ is the electrical conductivity and ε_r the relative dielectric permittivity. The advantage of having the conductivity depend upon the permittivity is that the number of parameters in the model is greatly reduced. (The rationale for this relation is in section 5.2.) The relative magnetic permeability was set to 1 in all layers. The current was chosen to be represented by an analytic function because such functions are simple; the best match was obtained with this exponentially-damped, sinusoidal function:

$$I(t) = \left(\frac{2\pi f_o t}{\sqrt{3}}\right)^2 \exp\left(-\frac{2\pi f_o t}{\sqrt{3}}\right) \sin(2\pi f_o t) u(t) \tag{2}$$

where t is time, f_0 is the dominant frequency, and u is the Heaviside step function (Chan and Tsang, 1983). The dominant frequency in the recorded scans is 70 MHz, and f_0 was set to this value too.

The relative dielectric permittivity and the constants in equation 1 were changed until the calculated scans matched the field scans. A match was deemed acceptable if the traveltime and the amplitude for a calculated scan were within 0.5 ns and about ten percent, respectively, of those for a field scan. The criterion involving traveltime was satisfied for all scans (Figure 7a); the criterion involving amplitude was satisfied for all scans except those near the middle. Furthermore, the trend in the percentage is similar to that in the relative dielectric permittivity (Figure 7c). These results suggest that a model with horizontal, homogeneous layers is adequate for modeling the radar data from the saturated zone; in other words, the sediments, to a first approximation, are horizontally-layered. As expected, this interpretation is similar to that for the unsaturated zone.

5.2 Discussion of Interpretation

The forward modeling was based, in part, on an assumed relation between the electrical conductivity and the relative dielectric permittivity. To determine whether such a relation exists indeed, extensive laboratory measurements would be required. As such an effort was far beyond the scope and the resources of this investigation, the relation was assumed. Nonetheless, the general trend inherent in the relation is believed to be correct: At Savannah River Site, the electrical conductivity is much higher in clay-rich layers than it is in clay-poor layers (Nelson and Kibler, 1996). Because the dielectric permittivity is higher in layers with a high percentage of clay-size particles than it is in layers with a low percentages (Figure 7), the conductivity and the permittivity appear to be indirectly related.

Even though the criteria for matching the calculated and the field scans was generally satisfied, in some cases the character of the two waves differ. For example, at 150.1 ft (45.75 m), the duration of the radar wave in the calculated scan is much longer than that in the field scan. Such differences exist because the model is not representing some field conditions like lateral changes in the sediments, frequency dependence in the constitutive parameters, the finite lengths of the antennas, changes in the electromagnetic properties of the grout, etc. Of these, I suspect that the first two are the most important. Despite the inadequacies of the model, the interpretation is consistent with the known geology.

6. GENERAL DISCUSSION

Because the random noise in the scans made the interpretation somewhat more difficult than it would have been otherwise, a cursory analysis of the noise was performed. Four properties of the noise are evident in some typical scans (Figure 8): (1) In the scans collected in the unsaturated zone and between the same pair of wells (top three scans in Figure 8a), the amount of noise is the same regardless of the depth. (2) In the scans collected in the unsaturated zone and at the same depth (bottom three scans in Figure 8a),

the amount of noise is practically the same regardless of the pair of wells between which the data were collected. (Although the amplitude of the noise in the scan for wells MSB-22 and MSB-3D is slightly greater than that in the other scans, this slight increase can be ignored for this analysis.) (3) The amplitude of the noise in the saturated zone is much less than that in the unsaturated zone. (4) In the scans from the saturated zone, the amount of noise at 132.9 ft, which is above a thick clay layer extending from 140 to 148 ft (Figure 5), is much greater than that at 150.1 ft, which is below the clay layer.

These observations are the basis of three hypotheses about the behavior of the noise: (1) The noise entered the well containing the receiving antenna, propagated along the well, and was detected by the antenna. (2) At the water table, most noise is reflected, making the amplitude of the noise in the saturated zone smaller than that in the unsaturated zone. (3) The noise is weakly affected by the properties of the sediments and the grout in the unsaturated zone, but it is strongly affected by these properties in the saturated zone. These hypotheses should be investigated further.

At the start of the investigation, tomography was thought to be an appropriate method for processing the data, and so the data were collected in a manner suitable for tomography: scans were recorded with the receiving antenna higher and lower than the transmitting antenna. In a typical example of data from the unsaturated zone (Figure 9), the radar wave is absent if the receiving antenna is more than a few feet higher or lower than the transmitting antenna. The radar waves in saturated zone behave similarly. The likely reason for the absence of the wave is that it is being completely attenuated by clays (Ellefsen, 1996). Although the absence of a wave is, in itself, information about the properties of the sediments, this information cannot be incorporated yet into modern tomographic processing; it can only be omitted from the processing, making the resolution of the tomographic images poor (Bregman and others, 1989). Consequently, modern tomographic methods are generally inadequate for processing crosswell radar data from Savannah River Site.

Although, in the unsaturated zone, the spacing between successive locations of the antennas would be suitable for processing and interpretation with tomographic methods, it was unsuitable for interpretation with forward modeling because the character of the waves in adjacent radar scans sometimes changes abruptly. The spacing would also be unsuitable for an inversion using the entire wave. Presently, no formula exists for calculating the necessary spacing; perhaps the spacing ought to be a fraction of the antenna lengths.

7. CONCLUSIONS AND RECOMMENDATIONS

Before this investigation, it was not known whether crosswell radar data could be collected at Savannah River Site — the sediments and the grout might attenuate the radar waves too much. The results unambiguously show that radar data can be collected and that the attributes of the waves are strongly related to the geology. Nonetheless, it is still

not known whether crosswell radar is a suitable means of monitoring DNAPL remediation; this can be determined only with a field test.

If a test is conducted, then these changes in data collection and processing are recommended: (1) The field procedures or equipment or both should be modified to diminish the random noise. (2) The spacing between successive radar scans should be decreased to a fraction of the antenna length. With denser spacing, it should be easier to map changes in lithology and perhaps to detect changes in pore fluids. (3) The electromagnetic properties of the wells and the sediments near the wells should be measured with a dielectric logging tool. These properties will constrain the interpretation of the radar data.

8. ACKNOWLEDGMENTS

D. Muller helped with the data collection, B. Pemberton organized all of the field support, and C. Eddy-Dilek coordinated the field work and provided the logging data. J. Rossabi and D. Wright reviewed this report and made many helpful suggestions. This work was sponsored by the Department of Energy under Interagency Agreement DE–AI09–91SR18222.

9. REFERENCES

Bregman, N. D., Bailey, R. C., and Chapman, C. H., 1989, Ghosts in tomography: The effects of poor angular coverage in 2-D seismic traveltime inversion: Canadian Journal of Exploration Geophysics, v. 25, p. 7–27.

Born, M., and Wolf, E., 1980, Principles of optics (6th ed.): New York, Pergamon Press Inc., 808 p.

Bouchon, M., 1981, A simple method to calculate Green's functions for elastic layered media: Bulletin of the Seismological Society of America, v. 71, no. 4. p. 959–971.

Chan, A. K., and Tsang, L., 1983, Propagation of acoustic waves in a fluid-filled borehole surrounded by a concentrically layered transversely isotropic formation: Journal of the Acoustical Society of America, v. 74, no. 5, p. 1605–1616.

Daniels, J. J., 1989, Fundamentals of ground penetrating radar: Proceedings of the Symposium on the Application of Geophysics to Engineering and Environmental Problems, Golden, Colorado, Environmental and Enginering Geophysical Society, p. 62–142.

Davis, J. L., and Annan, A. P., 1989, Ground penetrating radar for high-resolution mapping of soil and rock stratigraphy: Geophysical Prospecting, v. 37, p. 531–551.

Devore, J. L., 1982, Probability and statistics for engineering and the sciences: Monterey, California: Brooks/Cole Publishing Co., 640 p.

DiStefano, M., 1989, Soil characterization at the Savannah River plant: Mineralogy, Technical Services Report No. 1809–005–011–1–89, Conoco Exploration Research & Services, available from Environmental Sciences Section, Westinghouse Savannah River Company, Aiken, SC 29808

Eddy-Dilek, C. A., Looney, B. B., Hazen, T. C., Nichols, R. L., Fliermans, C. B., Parker, W. H., Dougherty, J. M., Kaback, D. S., and Simmons, J. L., 1993, Post-test evaluation of the geology, geochemistry, microbiology, and hydrology of the *in situ* air stripping demonstration site at the Savannah River Site, Report No. WSRC–TR–93–369, Westinghouse Savannah River Company, Aiken, SC 29808

Ellefsen, K. J., 1995, High resolution mapping of stratigraphy using seismic tomography: A feasibility test at the M-Area Basin, Savannah River Site, South Carolina: U. S. Geological Survey Open-File Report 95–518, 46 p.

Ellefsen, K. J., 1996, Cross-well radar in layered sediments: U. S. Geological Survey Open-File Report 96–510, 24 p.

Environmental Sciences Section, 1993, Microscopic examination of sediment cores, Manual WSRC–L14.1, Procedure 2–15, Rev.2, available from Environmental Sciences Section, Westinghouse Savannah River Company, Aiken, SC 29808

Geophysical Survey Systems, Inc., 1993, SIR^{TM} System–10A user's manual #MN90–305: North Salem, New Hampshire, Geophysical Survey Systems, Inc., various paginations.

Greenhouse, J., Brewster, M., Schneider, G., Redman, D., Annan, P., Olhoeft, G., Lucius, J., Sander, K., and Mazzella, A., 1993, Geophysics and solvents: The Borden experiment: The Leading Edge, v. 12, no. 4, p. 261–267.

Hoekstra, P., and Delaney, A., 1974, Dielectric properties of soils at UHF and microwave frequenecies: Journal of Geophysical Research, v. 79, no. 11, p. 1699–1708.

Horton, R. J. 1996, Laboratory studies of selected core samples from A/M Area, Savannah River Site, South Carolina: U. S. Geological Survey Open-File Report 96–699, 143 p.

Jordan, J. E., Looney, B. B., Rossabi, J., Bergren, C. L., 1993, Savannah River Site DNAPL Technical Program Plan, Report No. WSRC–TR–93–606, Westinghouse Savannah River Company, Aiken, SC 29808

Nelson, P. H., Kibler, J. E., 1995, Geophysical logs and groundwater chemistry in the A/M Area, Interim report, Savannah River Site, South Carolina: U. S. Geological Survey Open-File Report 95–507, 78 p.

Nelson, P. H., Kibler, J. E., 1996, Geophysical logs and groundwater chemistry in the A/M Area, Final report, Savannah River Site, South Carolina: U. S. Geological Survey Open-File Report 96–75, 25 p.

Neter, J., Wasserman, W., Kutner, M. H., 1983, Applied linear regression models: Homewood, Illinois, Richard D. Irwin, Inc., 547 p.

Seagull, M. P., 1992, Clay-size mineralogic studies of selected samples from the Upland unit, Tobacco Road sands, Dry Branch formation, and Santee formation, South Carolina, *in* Sedimentology and stratigraphy of the Upland Unit, Progress Report, December 2, 1992, available from University of South Carolina, Department of Geological Sciences.

Stratton, J. A., 1941, Electromagnetic theory: New York, McGraw-Hill Inc., 615 p.

Wait, J. R., 1962, Electromagnetic waves in stratified media: New York: MacMillian Co., 372 p.

Westinghouse Savannah River Company, 1992, Assessing DNAPL contamination, A/M-area, Savannah River Site: Phase I results, Report No. WSRC–RP–92–1302, available from Environmental Sciences Section, Westinghouse Savannah River Company, Aiken, SC 29808

APPENDIX

In this appendix, the equations needed for forward modeling of crosswell radar data (section 5.1) are derived.

The model, which is shown in Figure A1, consists of a stack of horizontal, homogeneous, isotropic layers. The top and the bottom layers of the stack are half-spaces. For the layer with the antennas, which will be called the "antenna layer," the dielectric permittivity is ε, the magnetic permeability is μ, the electrical conductivity is σ, and the thickness is h. A vertical electric dipole, which simulates the transmitting antenna, is at a distance z_t from the bottom of the antenna layer. The dipole moment is $I(\omega)\, ds / i\, \omega$ where $I(\omega)$ is the current, ds is the infinitesimal dipole length, ω is the angular frequency, and i is $\sqrt{-1}$. For this model, circular cylindrial coordinates for which the z axis is alligned with the dipole are appropriate; the model has azimuthal symmetry.

This model is similar to that used by Wait (1962, p. 182–183) who analyzed electromagnetic wave propagation in the atmosphere. Because the only difference is that in Wait's model the layer below the antenna layer was a half-space, the method of solution used by Wait can be used here too with some minor modification. Within the antenna layer, the electromagnetic field is expressed in the frequency-wavenumber domain via a Hertz potential Π that has only a z component:

$$\Pi(k_r, z, \omega) = -Mi \frac{e^{-ik_z|z-z_t|}}{k_z} + Ae^{ik_z z} + Be^{-ik_z z} \tag{A1}$$

where

$$M = \frac{I(\omega)ds}{4\pi(\sigma + i\omega\varepsilon)} \quad , \tag{A2}$$

k_z and k_r are the vertical and the radial components of the wave number, and A and B are coefficients. The first term in equation A1 represents the wave field radiated by the transmitting antenna; the second and the third terms represent another wave field caused by the interaction of the radiated wave field with the other layers in the stack.

The coefficients are calculated by matching the impedances, a procedure which is equivalent to matching the boundary conditions, on the top and the bottom of the antenna layer. The impedance caused by layers above the antenna layer is Z_U, which may be calculated using the formulas in Wait (1962, p. 11–12). This impedance must equal that caused by the fields within the antenna layer:

$$Z_U = \left. \frac{E_r(k_r, z, \omega)}{H_\varphi(k_r, z, \omega)} \right|_{z=h} . \tag{A3}$$

E_r is the radial component of the electric field intensity and is related to the Hertz potential via:

$$E_r(k_r,z,\omega)=\frac{\partial^2\Pi(k_r,z,\omega)}{\partial r\partial z}\,. \tag{A4}$$

H_φ is the azimuthal component of the magnetic field intensity and is related to the Hertz potential via:

$$H_\varphi(k_r,z,\omega)=N\frac{\partial\Pi(k_r,z,\omega)}{\partial r} \tag{A5}$$

where

$$N=\frac{k^2}{i\omega\mu} \tag{A6}$$

and k is the wave number. Equations A4 and A5 are substituted into equation A3, which is then integrated over r. Because the fields approach zero as r approaches ∞, the constant of integration is zero. The result is

$$\left.\frac{\partial\Pi(k_r,z,\omega)}{\partial z}\right|_{z=h}=Z_U N\Pi(k_r,z,\omega)\Big|_{z=h}\,. \tag{A7}$$

The derivation for the lower interface is identical, and the result is

$$\left.\frac{\partial\Pi(k_r,z,\omega)}{\partial z}\right|_{z=0}=Z_D N\Pi(k_r,z,\omega)\Big|_{z=0}\,. \tag{A8}$$

The expression for the potential (equation A1) is substituted into these two equations for the impedances to yield two simultaneous equations for the two unknown coefficients. The analytical solutions for the coefficients are

$$A=\frac{Mi}{k_z}\,\frac{e^{-2ik_z h}\dfrac{Z_U N+ik_z}{Z_U N-ik_z}\left(e^{ik_z z_1}-\dfrac{Z_D N-ik_z}{Z_D N+ik_z}e^{-ik_z z_1}\right)}{1-\dfrac{Z_U N+ik_z}{Z_U N-ik_z}\,\dfrac{Z_D N-ik_z}{Z_D N+ik_z}e^{-2ik_z h}} \tag{A9}$$

and

$$B=\frac{Mi}{k_z}\,\frac{\dfrac{Z_D N-ik_z}{Z_D N+ik_z}\left(e^{-ik_z z_1}-\dfrac{Z_U N+ik_z}{Z_U N-ik_z}e^{-2ik_z h}e^{ik_z z_1}\right)}{1-\dfrac{Z_U N+ik_z}{Z_U N-ik_z}\,\dfrac{Z_D N-ik_z}{Z_D N+ik_z}e^{-2ik_z h}}\,. \tag{A10}$$

Before the potential is used to derive any component of the electromagnetic field, the term for the radiated field will be modified because it causes numerical errors when z is close to z_t. To this end, apply the Fourier-Bessel transform to equation A1:

$$\Pi(r,z,\omega)=\int_0^\infty M\frac{e^{ik_z|z-z_t|}}{ik_z}J_0(k_r r)k_r dk_r+\int_0^\infty\left[Ae^{ik_z z}+Be^{-ik_z z}\right]J_0(k_r r)k_r dk_r \tag{A11}$$

The integral involving the radiated field, which is the Sommerfeld integral (Stratton, 1941, p. 576), is replaced by

$$M\frac{e^{ikR}}{R} \tag{A12}$$

where

$$R=\sqrt{r^2+(z-z_t)^2}\ . \tag{A13}$$

The vertical component of the electric field intensity, which is that component is sensed by the receiving antenna, is computed from the potential via

$$E_z(r,z,\omega)=\left(\frac{\partial^2}{\partial z^2}+k^2\right)\Pi(r,z,\omega)\ . \tag{A14}$$

After transformation to the time domain, the solution is

$$E_z(r,z,t)=\int_{-\infty}^{\infty}d\omega e^{i\omega t}\int_0^\infty\left[Ae^{ik_z z}+Be^{-ik_z z}\right]J_0(k_r r)k_r^3 dk_r+$$

$$\int_{-\infty}^{\infty}d\omega e^{i\omega t}Me^{-ikR}\left[\frac{3(z-z_t)^2}{R^5}+\frac{3ik(z-z_t)^2}{R^4}-\frac{k^2(z-z_t)^2+1}{R^3}-\frac{ik}{R^2}+\frac{k^2}{R}\right]. \tag{A15}$$

The integrals over radial wave number are computed via the discrete wave number method (Bouchon, 1981), and the integrals over frequency via fast Fourier transforms.

Table 1. Zero-offset data, which were collected in the wells on the north side of the M-Area basin (Figure 1).

Hydrologic Zone	Well with transmitting antenna	Well with receiving antenna	Spacing between successive locations of the antennas
unsaturated	MSB-3A	MSB-3B	1.6 ft (0.5 m)
unsaturated	MSB-3C	MSB-3A	1.6 ft (0.5 m)
unsaturated	MSB-3D	MSB-3C	1.6 ft (0.5 m)
unsaturated	MSB-22	MSB-3D	1.6 ft (0.5 m)
saturated	MSB-3C	MSB-3B	0.8 ft (0.25 m)

Table 2. Equipment settings used to collect the radar data.

Item	Setting (Unsaturated Zone)	Setting (Saturated Zone)
Duration of recording for each scan	100 ns	200 ns
Starting time for recording	10 ns	50 ns
Sample rate	0.1953 ns	0.1953 ns
Usual passband of filter	20-400 MHz	30-400 MHz

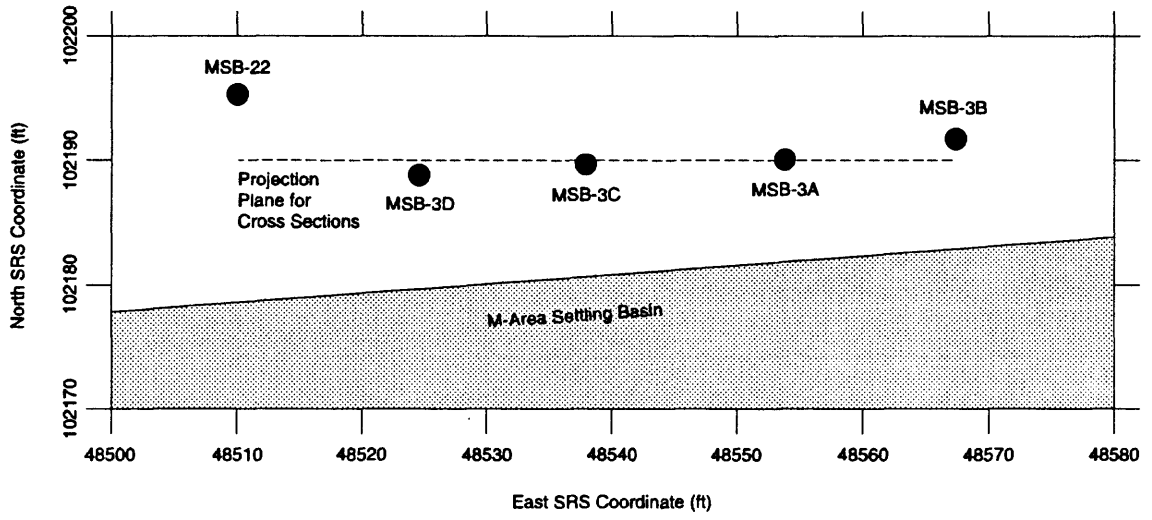

Figure 1. Wells in which the crosswell radar data were collected. The dotted line represents the location of the cross sections (Figures 2 and 5), into which the wells and the radar data were projected. Locations are specified in a planar coordinate system developed for Savannah River Site (SRS).

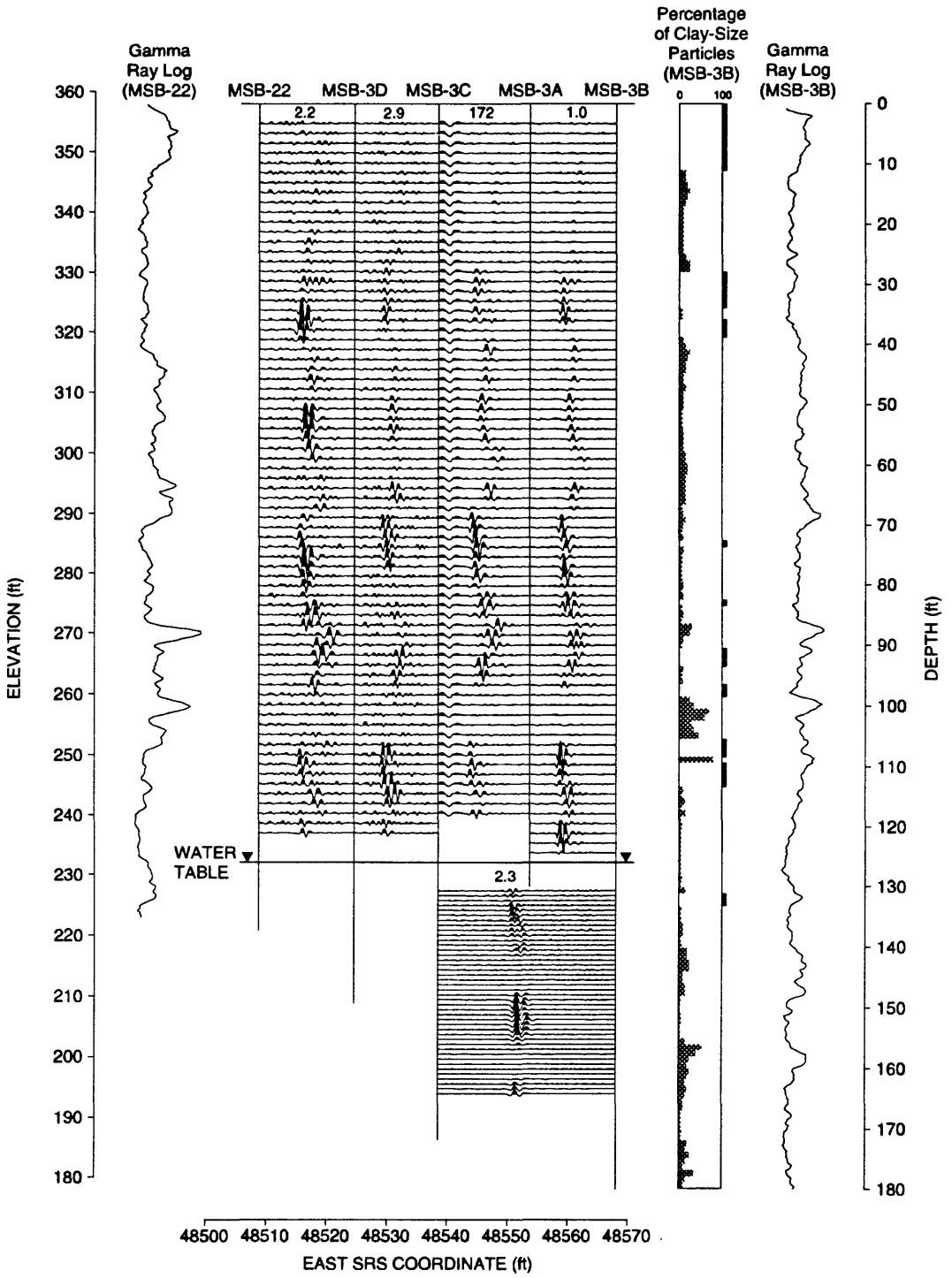

Figure 2. Crosswell radar data, percentage of clay-size particles, and gamma ray logs collected in the wells on the north side of the M-Area Basin. This cross section is along the east-west line shown in Figure 1. The format for plotting the data and the scaling factors are explained in section 3. In the log of the percentage, the solid bars on the right indicate where core was not recovered. Well MSB-3B extends beyond 180 ft (depth) — it was drawn to this depth only for the figure.

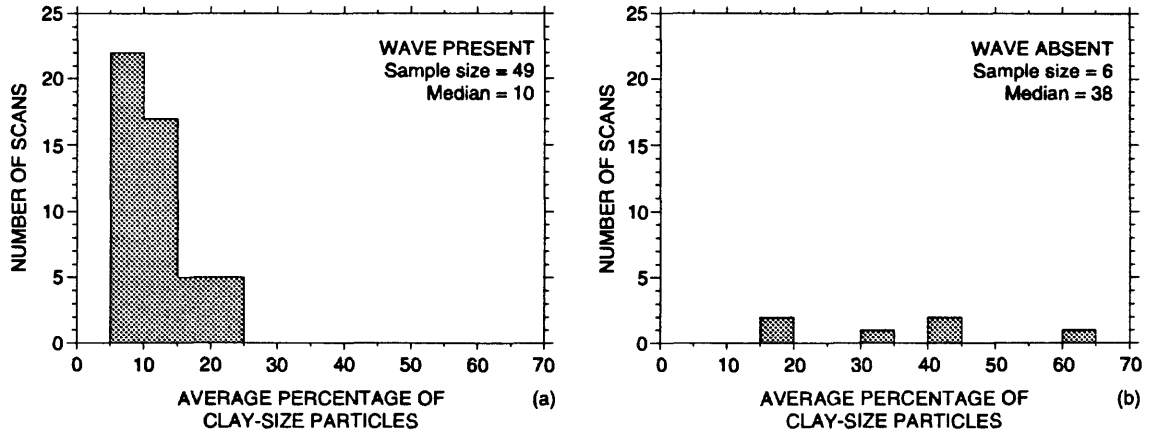

Figure 3. Histograms, for the unsaturated zone, showing the distribution of the average percentage of clay-size particles when the radar wave is (a) present and (b) absent. The percentages were measured in core extracted from well MSB-3B and then averaged over 3 ft (1 m) intervals. The radar data are between wells MSB-3A and MSB-3B.

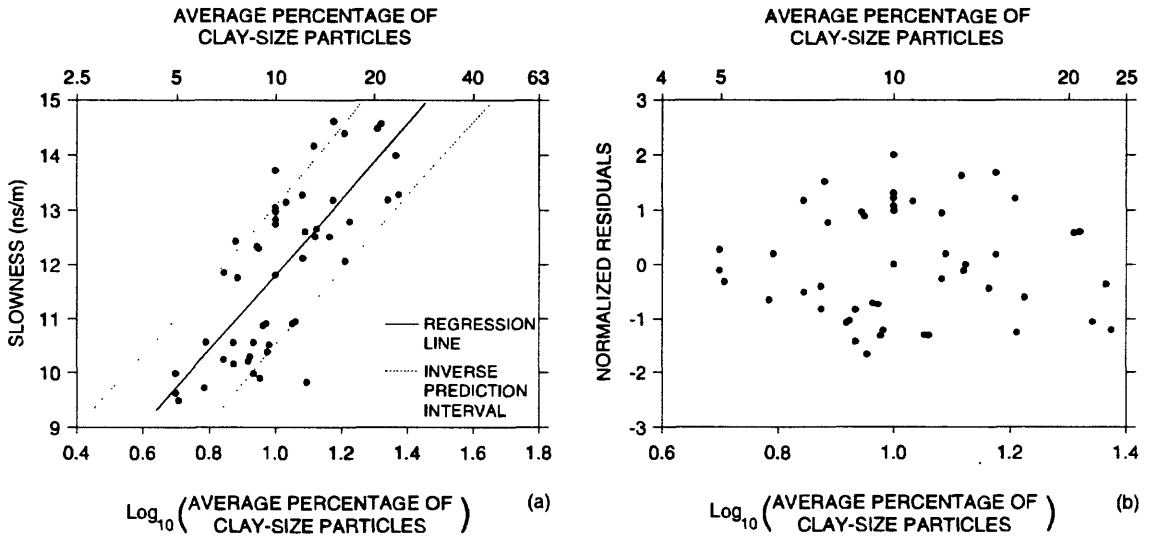

Figure 4. (a) Scatter plot with regression line and inverse prediction interval showing how the logarithm of the average percentage of clay-size particles is related to the slowness of a radar wave in the unsaturated zone. The percentages were measured in core extracted from well MSB-3B. The slownesses are from the radar data between wells MSB-3A and MSB-3B. (b) Normalized residuals showing the suitability of the linear model. Because of the normalization, one unit on the vertical axis is equivalent to the sample standard deviation.

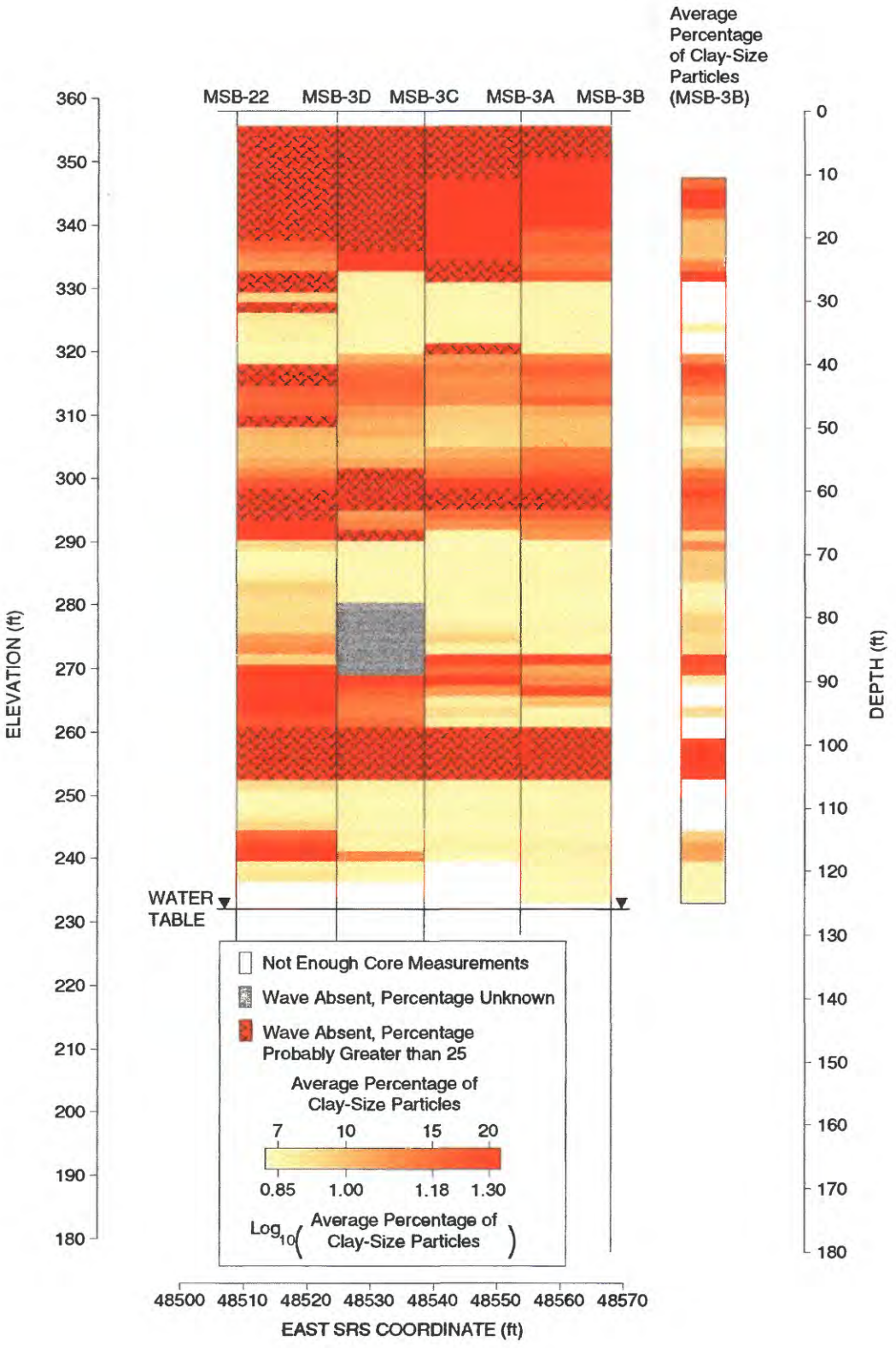

Figure 5. Predicted percentages of clay-size particles between the wells and average percentages for well MSB-3B. All percentages are on a logarithmic scale. At some depths, the average percentage could not be computed because the core measurements are too sparse. This cross section is along the east-west line shown in Figure 1.

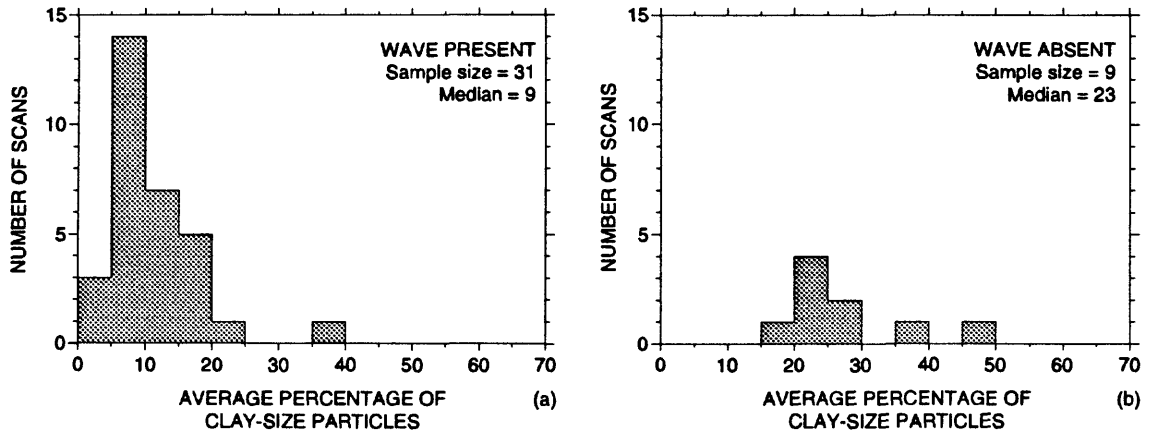

Figure 6. Histograms, for the saturated zone, showing the distribution of the average percentage of clay-size particles when the radar wave is (a) present and (b) absent. The percentages were measured in core extracted from well MSB-3B and then averaged over 3 ft (1 m) intervals. The radar data are between wells MSB-3C and MSB-3B.

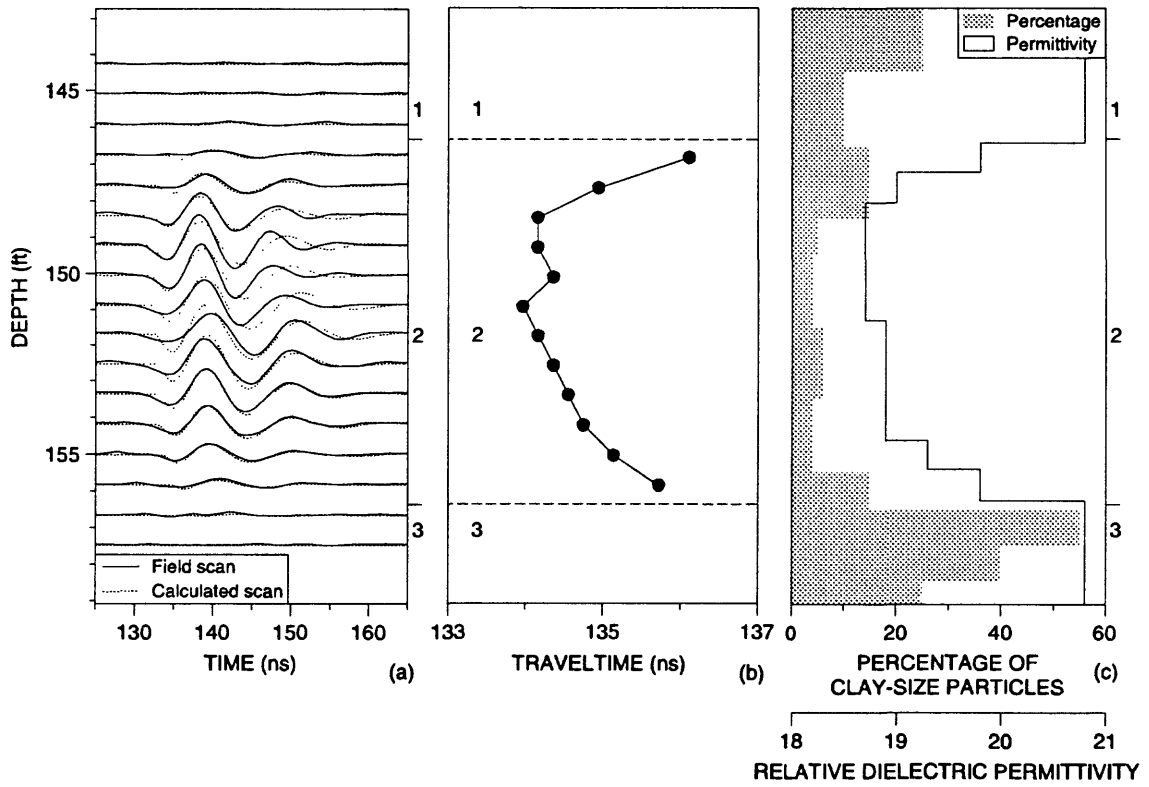

Figure 7. Forward modeling of data between 144 ft (44 m) and 158 ft (48 m) in the saturated zone. (a) Scans between wells MSB-3C and MSB-3B and calculated scans. The calculation of the scans is explained in section 5.1. (b) Traveltimes of the field scans in (a). (c) Percentage of clay-size particles for well MSB-3B and the relative dielectric permittivity used for forward modeling. The data were divided into three intervals indicated by the three numbers.

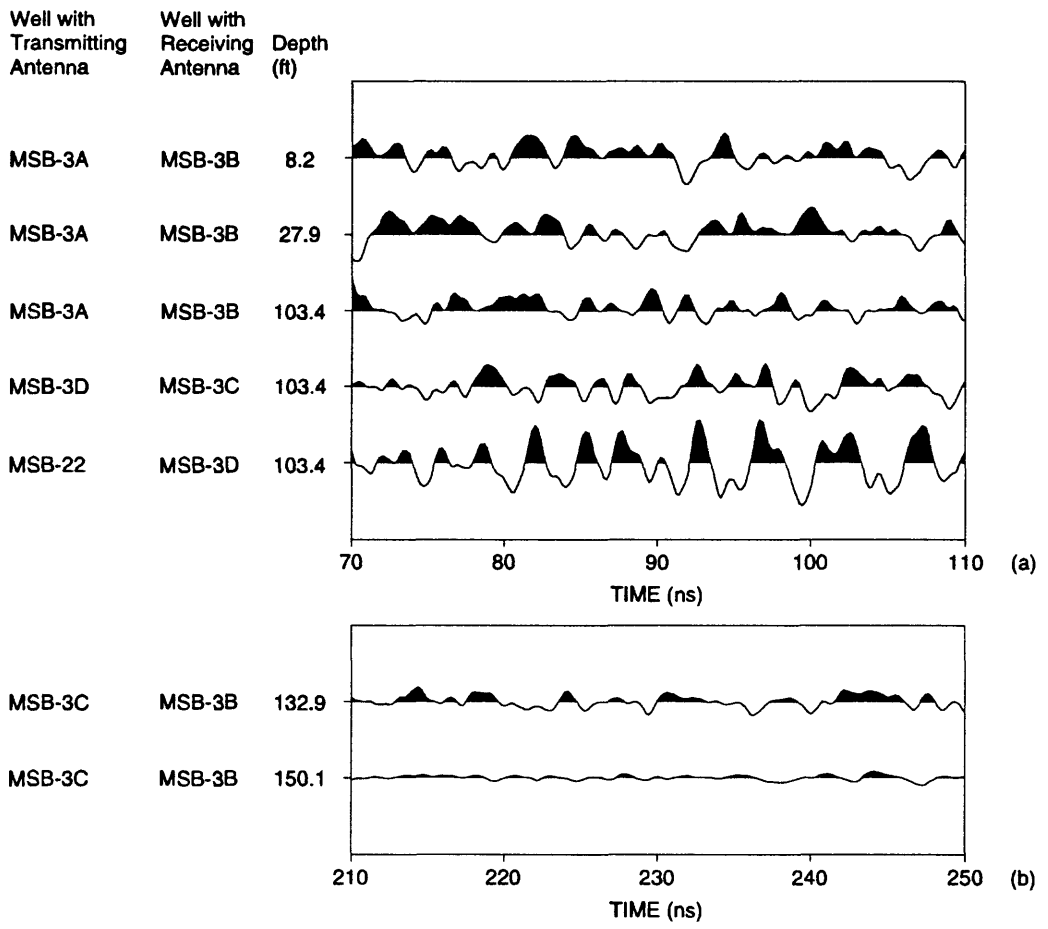

Figure 8. Typical noise in radar scans from (a) the unsaturated zone and (b) the saturated zone. The scaling was removed to make the scans readily comparable. Only the ends of the scans, after the arrival of the radar wave, are shown because the radar wave would complicate the analysis of the noise.

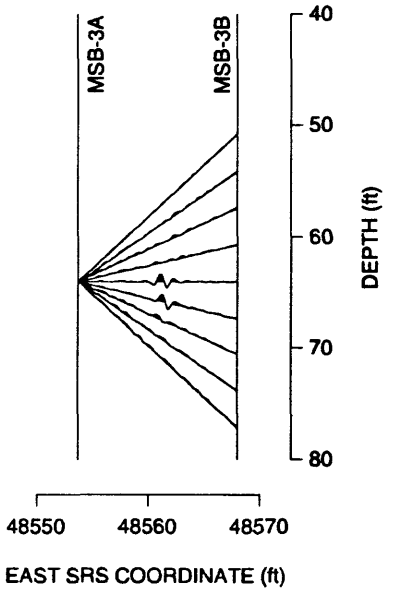

Figure 9. Typical data collected for tomography in the unsaturated zone. The beginning of each scan is on the left, at the location of the transmitting antenna; the end of each scan is on the right, at the location of the receiving antenna. The amplitudes were set to the same scale to make the scans readily comparable.

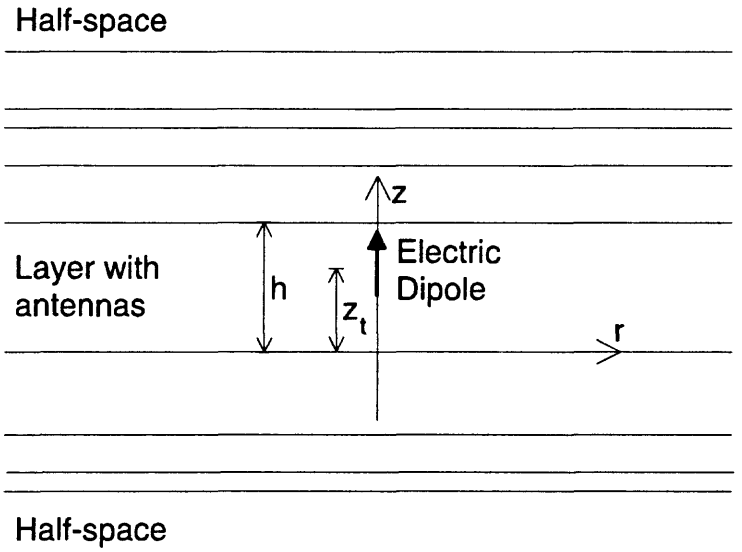

Figure A1. Model used to simulate radar wave propagation in layered sediments. The symbols are explained in the text.